

Computational modeling and simulation of rupture of membranes and thin films

Eduardo M. B. Campello

Received: 5 October 2013 / Accepted: 5 November 2014 / Published online: 30 November 2014
© The Brazilian Society of Mechanical Sciences and Engineering 2014

Abstract This paper presents a simple computational model for the rapid simulation of rupture on membranes and thin films. The proposed approach treats these surface structures as a collection of particles forming a discrete dynamical system, which is described by Newtonian equations in a purely mechanistic way. Detailed aspects about particle interactions are discussed and resolved. The main advantages of such an approach are that (1) it can offer a good picture of the dynamics of the rupture, yet resorting to only very simple descriptions of the underlying microstructure of the membrane or thin film, and (2) such different systems as structural fabrics, thin biological tissues and lipid membranes can be modeled under the same general framework. A time integration scheme is formulated for solution of the system dynamics, and examples of numerical simulations are provided. Computational particle-based models render reliable and fast simulation tools. We believe they can be very useful to study rupture phenomena on membranes and thin films.

Keywords Membranes and thin films · Structural fabrics · Fibrous biological tissues · Lipid membranes · Computational particle methods · Discrete element methods

Technical Editor: Lavinia Maria Sanabio Alves Borges.

E. M. B. Campello
Department of Structural and Geotechnical Engineering,
Polytechnic School, University of São Paulo, P.O. Box 61548,
São Paulo, SP 05424-970, Brazil

Present Address:
E. M. B. Campello (✉)
Department of Mechanical Engineering, University of California
at Berkeley, 6195 Etchevery Hall, Berkeley, CA 94720-1740, USA
e-mail: campello@usp.br; campello@berkeley.edu

1 Introduction

Membranes and thin films are important systems in modern engineering. They are observed in a number of applications and at varying length scales, such as roofing of large-span buildings, nautical sails, ballistic shields, airbags, solar panels, biosensors and biological membranes, to name just a few. Some of these surface entities (we mean “surface” in the sense that they are inherently two-dimensional structures) exhibit, below the (homogenized) continuum scale, a microstructure that consists of a network of either woven yarns or oriented fibers, as for example in structural fabrics or in thin, fibrous biological tissues. Some others are essentially a bi-dimensional assembly of macromolecules held together by short-range forces arising from weaker van der Waals, hydrophobic and hydrogen-bonding interactions, as in lipid membranes forming thin biofilms like Langmuir–Blodgett films and cell membranes. In all cases, although through different mechanisms, the underlying microstructure leads often to a strong anisotropic behavior at the meso or macro-scale, which is in turn difficult to describe mathematically—especially if one is interested in the prediction of damage and rupture of such entities.

In this context, the purpose of this work is to present a relatively simple, yet robust, computational model for the simulation of rupture on structural fabrics, biological tissues and lipid membranes. Remarkably, it can be used to model such different types of surface entities under the same general framework, the only requirement being that its parameters be taken according to the problem at hand. It can be numerically implemented with small effort by researchers interested in these fields, and may be tailored to specific applications very straightforwardly. We follow a purely mechanistic description (in the sense that chemical and biological aspects, if present, are not directly

addressed), keeping our focus only on the mechanical forces that dictate the response of the surface entity. This latter is treated as a collection of particles forming a discrete dynamical system, wherein each particle interacts with the others and the surrounding media via a complex combination of membrane forces due to weaving yarns/fibers or adhesive in-plane interactions, pressure and drag forces due to surrounding fluids, and contact and friction forces due to touching and collision. The presence of external bodies (e.g., indenters or incoming objects or projectiles) is taken into account by treating them also as particles or collections of particles, which then take part into the overall particle interactions. Classical Newtonian dynamics is adopted to describe the time evolution of the system, the (strongly coupled) equations of which are solved via an implicit time-stepping integration scheme. The overall framework falls in the class of particle-based methods (PBM) or discrete element methods (DEM), see e.g., [1–3]. (These methods originated from the seminal work of Cundall and Strack [4] in the late 1970s, in an attempt to study granular materials like soils and rocks, and have evolved since then into powerful numerical approaches to the modeling of a myriad of discrete systems such as powders [5], granular flows [6], polymers [7], colloids [8], crystals [9], swarms [10] and many others, to cite just a few; for an early history and nice overview, the reader is referred to [11–13].) Examples of numerical simulations are provided to show how the model works from a general perspective.

The proposed approach has origins in the ideas of Zohdi and co-workers [14–17], but differs from these in the sense that a PBM description is envisioned for the surface entity instead of the so-called “network representation” developed therein. To the author’s knowledge, there are no previous works in the literature that attempted to devise a unified model for the simulation of rupture of surface entities by means of particle-based or DEM approaches. This is found to be the main contribution of this work and its key advantages are that (1) self-contact of the surface entity is made possible (this can be an important feature in many applications); (2) multi-layered surface entities with consistent inter-layer interaction are possible to be represented (in this case, contiguous layers may interact with each other via a combination of contact, friction and/or adhesion forces that follow naturally from the PBM description); (3) no closest-point projection algorithm needs to be invoked to resolve the contact of incoming objects with the surface entity (since the corresponding contact/collision forces follow from simple overlap-based contact solutions or from simple impulse–momentum balance calculations for each colliding pair); and (4) the presence of a matrix or coating material that is part of the surface entity can be easily considered, allowing for an in-plane shear

stiffness within the entity’s overall mechanical response. This approach, however, is not free from limitations or disadvantages. As a main drawback, we can stress that a robust contact search and detection algorithm is necessary (and indeed of crucial importance), since the particle-based description assumes by default that all particles in the system may potentially interact and get in contact with each other, thereby requiring an intensive contact check (this operation is of the order of N_p^2 , with N_p being the total number of particles in the system). Many schemes are available to speed up this check, as for example sorting and binning algorithms [18], domain decomposition algorithms [2], use of Verlet lists [2], etc.

There exists a number of other theoretical and/or computational approaches that may be used to study the mechanical response of structural fabrics [19–28], fibrous biological tissues [15, 29–32] and lipid membranes [33–42] (to cite just a few). Yet, to properly represent anisotropic deformation and rupture at the meso- or macro-scales, we believe that particle-based models (and, to some extent, models based on the network representation of [14–17]) are among the most suited. They allow for a simple representation of the surface entity and external objects. Also, multiple contact/impact with the opening of localized holes on the surface (localized rupture) and material segregation are straightforward to characterize. They offer a good picture of the structure and dynamics of the rupture, yet requiring only simple descriptions of the entity’s underlying microstructure. They render rapid, reliable simulation tools with which both rate-dependent (e.g., impact-induced) and quasistatic rupturing are possible to be simulated. With such tools, membrane and thin film systems can be more thoroughly studied or tested without the need to resort to a great number of physical experiments. Physical experiments can be expensive and time consuming, and the number of parameters that can be adjusted within feasible cost and time is very limited when compared to computational investigations.

The paper is organized as follows: in Sect. 2, we present a brief description of the equations that govern the dynamics of particulate systems (with emphasis on the several types of mechanical forces that are needed to our model, and their possible representations); in Sect. 3 we explain how we model surface entities with a PBM description (this was done separately from Sect. 2 such that specific aspects could be addressed in more details); in Sect. 4 we introduce our numerical solution scheme to the system’s equations; in Sect. 5 we show examples of numerical simulations that were carried out in three model problems; and in Sect. 6 we conclude the paper with some remarks and ideas for future work.

Throughout the text, for the ease of expression, the generic term “membrane” will be used to refer

indistinguishably to structural fabrics, fibrous biological tissues or lipid membranes. Difference between these surface entities will be made only where necessary.

2 Dynamics of particulate systems

In this and the following sections, plain italic letters ($a, b, \dots, \alpha, \beta, \dots, A, B, \dots$) will represent scalar quantities, whereas boldface italic ones ($\mathbf{a}, \mathbf{b}, \dots, \boldsymbol{\alpha}, \boldsymbol{\beta}, \dots, \mathbf{A}, \mathbf{B}, \dots$) will denote vectors in a three-dimensional Euclidean space. The (standard) inner product of two such vectors \mathbf{u} and \mathbf{v} will be indicated by $\mathbf{u} \cdot \mathbf{v}$, and the norm of a vector by $\|\mathbf{u}\| = \sqrt{\mathbf{u} \cdot \mathbf{u}}$.

We assume that all particles are spherical and that they are small enough so that the effect of their rotations with respect to their center of mass is unimportant to their overall motion. Moreover, they are considered to be elastic and quasi-rigid, in the sense that they neither undergo permanent nor large deformations when in contact with other particles. This means that they remain spherical and with constant radius at all times. Effects of temperature changes and associated heat transfer are also considered to be irrelevant, although these can be easily incorporated, following for example the coupled, multifield scheme proposed in [43].

Let our system comprise N_p particles, each one with known mass m_i and known radius R_i . We denote the position vector of particle i by \mathbf{r}_i , the velocity vector by \mathbf{v}_i and the acceleration vector by \mathbf{a}_i . According to Newton’s second law, at every time instant t the following equation must hold for each particle:

$$m_i \mathbf{a}_i = \mathbf{f}_i^{\text{tot}}, \tag{1}$$

where $\mathbf{f}_i^{\text{tot}}$ is the total force vector acting on the particle. This vector is made up of the sum of four force contributions as follows:

$$\mathbf{f}_i^{\text{tot}} = \mathbf{f}_i^{\text{env}} + \mathbf{f}_i^{\text{memb}} + \mathbf{f}_i^{\text{con}} + \mathbf{f}_i^{\text{fric}}, \tag{2}$$

in which $\mathbf{f}_i^{\text{env}}$ comprises the forces due to the environment acting on the particle (it represents the effects of the surrounding media on the particle), $\mathbf{f}_i^{\text{memb}}$ the forces due to membrane “in-plane” connections or interactions with other membrane particles (in case i is a particle of the membrane) (it represents the effects of weaving yarns in a structural fabric, or tissue fibers in a biological tissue, or intermolecular binding interactions in a lipid membrane), $\mathbf{f}_i^{\text{con}}$ the forces due to mechanical contact or collisions with other particles (and/or with obstacles), and $\mathbf{f}_i^{\text{fric}}$ the forces due to friction that arise from these contacts or collisions.

For the forces due to the environment, we write

$$\mathbf{f}_i^{\text{env}} = m_i \mathbf{g} + \mathbf{f}_i^{\text{pres}} + \mathbf{f}_i^{\text{drag}}, \tag{3}$$

where \mathbf{g} is the external gravity field, and $\mathbf{f}_i^{\text{pres}}$ and $\mathbf{f}_i^{\text{drag}}$ are the pressure and drag forces due to the surrounding fluid (e.g., air, water, aqueous solution, etc.). The pressure force is a given value or follows a given distribution, whereas the drag force is usually dependent on the particle’s velocity relative to the fluid (several expressions are possible depending on the characteristics of the flow, see e.g., [44]). Here, we adopt the following simple model, which constitutes a source of damping for the system:

$$\mathbf{f}_i^{\text{drag}} = -c_{\text{env}}(\mathbf{v}_i - \mathbf{v}_{\text{env}}), \tag{4}$$

in which c_{env} is a damping parameter and \mathbf{v}_{env} is the (local) velocity of the surrounding fluid. This is a one-way kind of coupling between the fluid and the particle, in the sense that the fluid affects the particle but the particle does not affect the fluid. More elaborately, fully coupled models can be constructed if necessary (although this increases the complexity of the solution scheme, since it introduces the fluid velocity and pressure fields as additional variables). Other environmental forces may be considered in (3), such as electric forces due to external electric fields, magnetic forces due to external magnetic fields, etc. We will comment briefly on this in Sect. 6.

For the forces due to membrane connections or interactions with other membrane particles, we write

$$\mathbf{f}_i^{\text{memb}} = \sum_{j=1}^{N_{\text{connec}}} \mathbf{f}_{ij}^{\text{memb}}, \tag{5}$$

where N_{connec} is the number of particles that are connected to particle i and $\mathbf{f}_{ij}^{\text{memb}}$ is the (binary) connecting force that acts between particle i and particle j . This force has the general form

$$\mathbf{f}_{ij}^{\text{memb}} = K_{ij} \mathbf{n}_{ij}, \tag{6}$$

in which K_{ij} is a scalar quantity dictating the intensity of the connection for the pair $\{i, j\}$ and \mathbf{n}_{ij} is the unit vector that points from the center of particle i to the center of particle j , i.e.,

$$\mathbf{n}_{ij} = \frac{\mathbf{r}_j - \mathbf{r}_i}{\|\mathbf{r}_j - \mathbf{r}_i\|} \tag{7}$$

(this vector will be from now on be referred to as the pair’s central direction). Scalar K_{ij} can be modeled in a number of ways, depending on the characteristics of the membrane, such as by using one-dimensional constitutive equations, or by using a combination of attractive and repulsive force coefficients that are functions of the distance between the particles [43] (this can be understood as derived from a generalized Mie’s potential, of which the classical Lennard-Jones potential [45] is a type), by using surface energy arguments [46, 47], direct van de Waals effects, etc. In

Sect. 3, we present the model that we have devised for the purpose of this work, which is based on the presence of a spring–dashpot device connecting particles i and j .

For the forces due to contact and collisions with other particles, there exist two classes of models that may be invoked, namely the overlap-based model and the impulse-based model. The adoption of one or the other must be dictated by the type of contact/collision that is expected to happen between the particles in the system. The overlap-based model is better suited when the contact involves relatively soft particles (yet rigid enough as to guarantee small contact deformations) and/or situations of enduring contact. In these cases, it is assumed that the contact force is a function of the amount of penetration (i.e., deformation) of the particles in contact, with the overlap between these particles considered as the magnitude of the penetration. This means that the deformation has to be resolved, and some constitutive equation is thereby necessary. The assumption of no permanent deformations due to collisions, stated at the beginning of this section, enables us to use the Hertz’s elastic contact theory (see [48]) to this end. Accordingly, based on Hertz’s solution, here we adopt the following expression for f_{ij}^{con} :

$$f_i^{con} = \sum_{j=1}^{N_c} f_{ij}^{con}, \tag{8}$$

$$f_{ij}^{con} = \frac{4}{3} \sqrt{R^* E^*} \delta^{3/2} n_{ij} + d \dot{\delta} n_{ij} \quad (\text{overlap-based model}),$$

where N_c is the number of particles that are in contact with particle i , f_{ij}^{con} is the (binary) contact force that acts between the contacting pair $\{i, j\}$,

$$R^* = \frac{R_i R_j}{R_i + R_j} \quad \text{and} \quad E^* = \frac{E_i E_j}{E_j(1 - \nu_i^2) + E_i(1 - \nu_j^2)} \tag{9}$$

are the effective radius and the effective elasticity modulus of the contacting pair (in which E_i, E_j and ν_i, ν_j are the elasticity modulus and the Poisson coefficient of particles i and j , respectively),

$$\delta = \|\mathbf{r}_i - \mathbf{r}_j\| - (R_i + R_j) \tag{10}$$

is the penetration (or overlap) between the pair in the pair’s central direction, $\dot{\delta}$ is the rate of this penetration (the superposed dot denotes differentiation with respect to time), and d is a damping constant that is introduced to allow for some energy dissipation. Figure 1 provides an illustration of a colliding pair.

The impulse-based model, on its turn, is better suited when the contact involves relatively stiff spheres that do not remain in contact after the collision has come to an end. In this case, the collision is an almost instantaneous (i.e., of

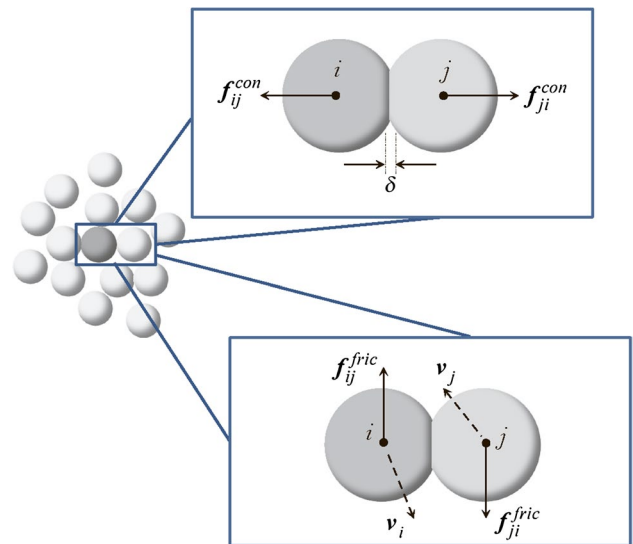


Fig. 1 Contact/collision between two particles

very small duration) event, and a simple balance of linear momentum before and after it is sufficient to compute the forces involved. Accordingly, we adopt here the following expression for these cases:

$$f_i^{con} = \sum_{j=1}^{N_c} f_{ij}^{con}, \tag{11}$$

$$f_{ij}^{con} = \bar{I}_n n_{ij} \quad (\text{impulse-based model}),$$

where \bar{I}_n is the (averaged) impulsive force exerted by the colliding pair over each other in the pair’s central direction during the collision, obtained as shown in the “Appendix” and given by

$$\bar{I}_n = \frac{1}{\delta t} \int_{t^*}^{t^* + \delta t} I_n dt = \frac{m_i(v_{in}(t^* + \delta t) - v_{in}(t^*))}{\delta t} - \bar{f}_{in}. \tag{12}$$

Here, t^* is the time instant at the beginning of the collision, δt is the duration of the collision,

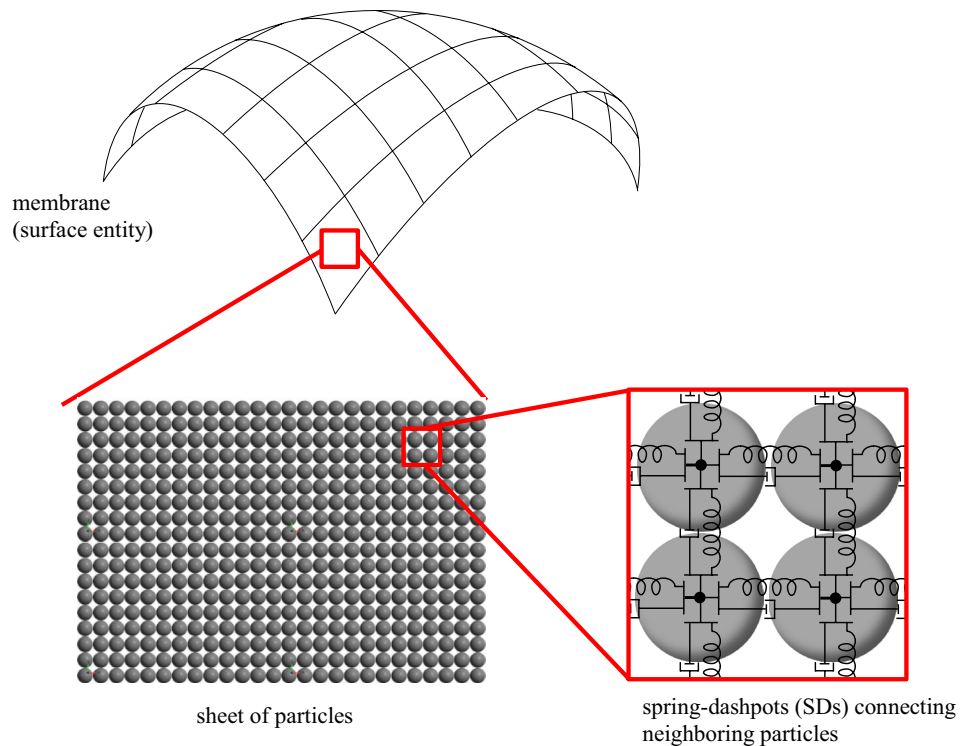
$$v_{in}(t^*) = \mathbf{v}_i(t^*) \cdot \mathbf{n}_{ij} \quad \text{and} \quad v_{in}(t^* + \delta t) = \mathbf{v}_i(t^* + \delta t) \cdot \mathbf{n}_{ij} \tag{13}$$

are the components of particle i ’s velocity in the pair’s central direction immediately before and after the collision, and

$$\bar{f}_{in} = \frac{1}{\delta t} \int_{t^*}^{t^* + \delta t} (f_i^{env} + f_i^{memb} + \sum_{k \neq j} f_{ik}^{con} + f_i^{fric}) \cdot \mathbf{n}_{ij} dt \tag{14}$$

is the (averaged) resultant force that act on particle i during the collision in the pair’s central direction as a result

Fig. 2 Membrane model: the membrane is idealized as a “sheet” of interconnected particles



of all other forces that act on i except for the pair’s contact force itself. The post-collision velocity $v_{in}(t^* + \delta t)$ is computed from the coefficient of restitution of the colliding pair (see the “Appendix”), which must be known a priori. One important aspect in this model is that, when solving the system’s dynamics by a time discretization/integration scheme, one finds that the adopted time steps Δt are typically much larger than the collision duration. This requires one to “smear out” the contact forces over the whole time step, by multiplying them by a factor $\delta t/\Delta t$. Additionally, the value of δt is usually not known and must be arbitrarily chosen for the forces to be computed. A typical choice is $\delta t = \gamma \Delta t$, with $\gamma = 0.01$ (normally, the model is insensitive to γ below 0.01, as demonstrated in [43]).

For the forces due to friction, which arise from the contacts/collisions, we assume that the friction coefficients are small enough so that a continuous slide, with an opposing dynamic friction force, is to be expected during the entire contact/collision (see Fig. 1). By “continuous slide” we mean that there is no stick between the contacting pair. Although a stick–slip model can also be considered, it is unnecessary for the types of problems that we are concerned with in this work. Thereby, here we write

$$\begin{aligned}
 \mathbf{f}_i^{\text{fric}} &= \sum_{j=1}^{N_c} \mathbf{f}_{ij}^{\text{fric}}, \\
 \mathbf{f}_{ij}^{\text{fric}} &= \mu_d \left\| \mathbf{f}_{ij}^{\text{con}} \right\| \boldsymbol{\tau}_{ij} \quad (\text{continuous slide model}),
 \end{aligned}
 \tag{15}$$

where $\mathbf{f}_{ij}^{\text{fric}}$ is the (binary) friction force that acts between particle i and particle j , μ_d is the coefficient of dynamic friction for the colliding pair, and

$$\boldsymbol{\tau}_{ij} = \frac{\mathbf{v}_{jt} - \mathbf{v}_{it}}{\|\mathbf{v}_{jt} - \mathbf{v}_{it}\|}
 \tag{16}$$

is the tangential direction of the contact/collision, which is the direction of the tangential relative velocity, computed as above with

$$\begin{aligned}
 \mathbf{v}_{it} &= \mathbf{v}_i - (\mathbf{v}_i \cdot \mathbf{n}_{ij}) \mathbf{n}_{ij} \\
 \mathbf{v}_{jt} &= \mathbf{v}_j - (\mathbf{v}_j \cdot \mathbf{n}_{ij}) \mathbf{n}_{ij}.
 \end{aligned}
 \tag{17}$$

3 Particle-based membrane model

We idealize the membrane as a collection of particles forming a bi-dimensional “sheet” or “layer”, in which each particle is connected to its immediate neighboring ones by means of fictitious spring–dashpots (SDs), as indicated in Fig. 2. Each SD provides an “in-plane” or “in-layer” membrane force $\mathbf{f}_{ij}^{\text{memb}}$ between particles i and j of the sheet, with $\mathbf{f}_{ij}^{\text{memb}} = -\mathbf{f}_{ji}^{\text{memb}}$, and is characterized by a stiffness constant k_{ij} , a damping constant c_{ij} and an initial length L_{ij}^0 .

If the membrane is a structural fabric, the SDs may be understood as elements representing the weft and warp yarns of the weave network, with the particles being lumped masses that provide thickness and inertia to the sheet. The diameter of the particles can be taken as the sheet’s thickness, and their masses as following a

consistent lumping from the sheet's (known) total mass. If the membrane is a biological tissue, the SDs can be thought of as representing the fibers of the tissue. In this case, the arrangement of the particles within the layer may be constructed so as to reproduce any preferential orientation of the tissue. The SDs' stiffnesses may be considered with different values for each direction, according to this preferential orientation, whereas the diameter and the mass of the particles can be taken similarly as to structural fabrics. If the membrane is a lipid membrane, the SDs can be understood as fictitious entities representing the overall (average) effects of the intermolecular forces that are observed at the "micro"-scale between two neighboring lipid molecules. In this case, k_{ij} and c_{ij} are "homogenized" properties representing the short-range attractive/repulsive interactions between the polar headgroups and the hydrocarbon chains of the neighboring lipids. This idealization was introduced by the author in the context of cell membranes in a recent contribution [36, 37], and proved to work very well in capturing the overall dynamical behavior of bi-lipid layers. In fact, the author believes that many of the physical properties of lipid membranes can be qualitatively described without the need to resort to detailed representations of the complex intermolecular interactions that are involved. In an analogy with gas-liquid phase interactions in thermodynamics, for example, the classical van der Waals equation of state contains no information on the characteristics and range of intermolecular forces, and yet renders a very satisfactory representation of the phase behavior.

With such a scheme, on each particle i of the membrane there act N_{connec} in-layer membrane forces, corresponding to the N_{connec} SDs that are connected to it. This allows us to write, for each of these particles:

$$\mathbf{f}_i^{\text{memb}} = \sum_{j=1}^{N_{\text{connec}}} \mathbf{f}_{ij}^{\text{memb}}, \quad (18)$$

$$\mathbf{f}_{ij}^{\text{memb}} = k_{ij} \Delta L_{ij} \mathbf{n}_{ij} - c_{ij} (v_{in} - v_{jn}) \mathbf{n}_{ij},$$

where

$$\Delta L_{ij} = \|\mathbf{r}_i - \mathbf{r}_j\| - L_{ij}^0 \quad (19)$$

is the elongation of the spring that connects the pair $\{i, j\}$ and

$$v_{in} = \mathbf{v}_i \cdot \mathbf{n}_{ij} \quad \text{and} \quad v_{jn} = \mathbf{v}_j \cdot \mathbf{n}_{ij} \quad (20)$$

are the central components of the pair's velocities \mathbf{v}_i and \mathbf{v}_j , respectively. To allow for the connections to break (rupture) if the particles are pulled apart strongly enough, we provide each SD with a critical strain $\varepsilon_{ij}^{\text{crit}}$, that leads to a critical elongation $\Delta L_{ij}^{\text{crit}}$. Once this critical value is reached, the

corresponding SD is turned off, that is, it does not enter the summation in Eq. (18).

Multi-layered membranes can be constructed straightforwardly by piling single layers on top of each other, and then placing transverse (or "through-the-thickness") additional SDs connecting each layer with its adjacent one(s). Also, in-layer shear-resistant membranes (e.g., membranes to which a matrix or a coating material provides an in-layer shear stiffness) can be modeled, by introducing in-plane cross-wise SDs. The cross-wise arrangement is simple yet consisted a way to enable the membrane an in-layer shear stiffness. This is of paramount importance in problems involving membrane shearing.

One important issue in such model is how to come up with proper values for the springs' stiffnesses. In case of structural fabrics and biological tissues, they can be taken with minor difficulties from physical experimental tests. In case of lipid membranes, however, these tests are usually more intricate and time consuming (although possible, see e.g., [49, 50], and references therein). We suggest then that they be estimated from surface tension or surface energy arguments, since the value of the surface tension (or interfacial free energy per unit area) for lipid-aqueous interfaces is well documented in the literature. This is reported as being around 50 mJ/m² for phospholipid monolayers. The interested reader on the physics of this topic is referred to [51] and the many works that followed, and also to the comprehensive work of [47].

One should notice that the approach proposed in this section, i.e., the use of spring-dashpots to represent membrane connecting forces (i.e., "bonding") between particles, can be used in a number of other problems whenever a pair-wise connection is to be established. The only requirement is that the SDs be judiciously placed according to the problem at hand, so as to capture the desired connected or "bonded" motion of the corresponding particles. Also, since in the approach each individual connection is assumed to behave according to a one-dimensional constitutive relation, more complex laws such as nonlinear hyperelasticity with progressive damage and rupture (allowing for non-abrupt breaking), or elastoplasticity, can be straightforwardly incorporated. The approach also constitutes a very simple way to implement pair-wise interactions, since every connecting/bonding pair has to be explicitly declared.

Remark 1 The use of dashpots in this idealization allows us to capture "in-plane" or "in-layer" viscous effects in a very simple way. This is a very important feature in some applications, as for example in the impact of high-speed incoming objects, or in dynamic tearing. Also, the behavior of extremely viscous materials such as lipid membranes becomes possible to be represented in a simple way.

Remark 2 For the modeling of initially curved membranes, description of the initial geometry can be pursued in a number of ways, as for example: (1) by using analytical surface equations to assign positions to particles’ centers; (2) by using CAD tools to generate a (spline or related) surface and then points belonging to this surface which would be particles’ centers; (3) by using FEM surface meshes whose nodes would be taken as particles’ centers, etc. This latter strategy, in particular, is very appealing due to its versatility and to the fact that FEM mesh generators are within easy reach to almost anyone in the computational mechanics community.

Remark 3 It could be argued that the compressive response of membranes on its in-layer directions should be enforced to zero, as in the relaxed theory of perfectly elastic solids (see Pipkin [52] for early mathematical accounts on this theory). This is suggested by many authors when dealing with continuum mechanics models for thin elastic membranes. In these cases, Steigmann and co-workers [53, 54] have demonstrated that a necessary condition for the existence of energy minimizers is that the structural members carry no load in compression. While this assumption could be readily incorporated into our model [by enforcing $k_{ij} = 0$ whenever $\Delta L_{ij} < 0$ in Eq. (18)], here instead we have no reasons nor need to neglect such effects. Indeed, one could go even further in our model and improve it by adopting different values for the compressive and tensile stiffnesses of the connections. This can be useful for example in the modeling of some types of biological tissues, wherein a very dissimilar response to tension and compression is known to exist and is believed to be the key to understanding their dynamic loading. Similarly, if cross-wise springs are used, different values for their stiffnesses (when compared to the non-cross-wise ones) can be considered.

4 Time integration scheme for solution of the system’s dynamics

To resolve the system dynamics, we start by considering the acceleration vector of each particle, which may be computed from Eq. (1). This vector is related to the particle’s velocity by the time-continuous differential equation

$$\frac{d\mathbf{v}_i}{dt} = \mathbf{a}_i. \tag{21}$$

Integration of this equation between time instants t and $t + \Delta t$, together with (1), furnishes

$$\mathbf{v}_i(t + \Delta t) = \mathbf{v}_i(t) + \frac{1}{m_i} \int_t^{t+\Delta t} \mathbf{f}_i^{\text{tot}} dt. \tag{22}$$

The integral in (22) is difficult (if not impossible) to be evaluated analytically because of the intricate variation of $\mathbf{f}_i^{\text{tot}}$ with time. A numerical approximation is thus necessary and here we adopt the following scheme, which corresponds to the use of a generalized trapezoidal rule:

$$\int_t^{t+\Delta t} \mathbf{f}_i^{\text{tot}} dt \approx [\phi \mathbf{f}_i^{\text{tot}}(t + \Delta t) + (1 - \phi) \mathbf{f}_i^{\text{tot}}(t)] \Delta t, \tag{23}$$

with $0 \leq \phi \leq 1$. If $\phi = 0$, the integration corresponds to an (explicit) forward Euler scheme; if $\phi = 1$, to an (implicit) backward Euler one; and if $\phi = 0.5$, to the (implicit) classical trapezoidal rule. By inserting (23) into (22), one has

$$\mathbf{v}_i(t + \Delta t) = \mathbf{v}_i(t) + \frac{\Delta t}{m_i} [\phi \mathbf{f}_i^{\text{tot}}(t + \Delta t) + (1 - \phi) \mathbf{f}_i^{\text{tot}}(t)]. \tag{24}$$

On the other hand, the velocity vector of each particle is related to the particle’s position by the time-continuous differential equation

$$\frac{d\mathbf{r}_i}{dt} = \mathbf{v}_i. \tag{25}$$

This equation can also be integrated between t and $t + \Delta t$, yielding

$$\mathbf{r}_i(t + \Delta t) = \mathbf{r}_i(t) + \int_t^{t+\Delta t} \mathbf{v}_i dt. \tag{26}$$

The integral on the right side of (26) is also difficult to be evaluated analytically, and then we adopt the following approximation, similarly to what was done in (23):

$$\int_t^{t+\Delta t} \mathbf{v}_i dt \approx [\phi \mathbf{v}_i(t + \Delta t) + (1 - \phi) \mathbf{v}_i(t)] \Delta t. \tag{27}$$

By introducing (27) into (26), one arrives at

$$\mathbf{r}_i(t + \Delta t) = \mathbf{r}_i(t) + [\phi \mathbf{v}_i(t + \Delta t) + (1 - \phi) \mathbf{v}_i(t)] \Delta t. \tag{28}$$

Expressions (24) and (28) constitute a set of equations for $i = 1, \dots, N_p$ particles, with which the velocity and position vectors of each particle at $t + \Delta t$ may be computed once $\mathbf{v}_i(t)$ and $\mathbf{r}_i(t)$ are known. This computation, however, cannot be performed directly, since (24) requires the evaluation of $\mathbf{f}_i^{\text{tot}}(t + \Delta t)$, which is in turn a function of all (!) unknown position and velocity vectors $\mathbf{r}_j(t + \Delta t)$ and $\mathbf{v}_j(t + \Delta t)$:

$$\begin{aligned} \mathbf{f}_i^{\text{tot}}(t + \Delta t) &= \hat{\mathbf{f}}_i^{\text{tot}}(\mathbf{r}_1(t + \Delta t), \mathbf{r}_2(t + \Delta t), \dots, \mathbf{r}_{N_p}(t + \Delta t), \\ &\quad \mathbf{v}_1(t + \Delta t), \mathbf{v}_2(t + \Delta t), \dots, \mathbf{v}_{N_p}(t + \Delta t)) \\ &= \hat{\mathbf{f}}_i^{\text{tot}}(\mathbf{r}_j(t + \Delta t), \mathbf{v}_j(t + \Delta t)), \quad j = 1, 2, \dots, N_p. \end{aligned} \tag{29}$$

This fact means that all equations are strongly coupled, and a recursive solution is thereby necessary. We adopt here a fixed-point iterative scheme, whose main steps are as summarized in (30). The scheme is relatively easy to be

implemented and it is noteworthy that no system matrix is required. Moreover, adaptivity of the time step size can be straightforwardly incorporated. One can prove that such kinds of schemes are convergent by realizing that they involve a contraction mapping for all $\mathbf{r}_i^{K+1}(t + \Delta t)$ (K being the iteration counter). Details on this aspect can be found in [43, 55].

Remark 6 The imposition of “boundary conditions” is very straightforward in this sort of particle model. Actually, the terminology “boundary conditions” is employed indistinguishably to refer two types of constraints within the DEM context: (1) geometrical boundaries or limits on the spatial domain and (2) constraints on positions and/or velocities of some particles, i.e., fixed (a priori-imposed)

GIVEN QUANTITIES: $t = 0$, $\Delta t = \text{known}$, $\phi = \text{known}$, $\mathbf{r}_i(t)$, $\mathbf{v}_i(t) = \text{known}$;

(1) INITIALIZE TIME - STEP :

$K = 0$ (iteration counter)

$\mathbf{r}_i^K(t + \Delta t) = \mathbf{r}_i(t)$, $\mathbf{v}_i^K(t + \Delta t) = \mathbf{v}_i(t)$ (predictor)

(2) FOR $i = 1, N_p$:

$$\begin{cases} \mathbf{f}_i^{\text{tot},K+1}(t + \Delta t) = \mathbf{f}_i^{\text{tot}}(\mathbf{r}_j^K(t + \Delta t), \mathbf{v}_j^K(t + \Delta t)) \\ \mathbf{v}_i^{K+1}(t + \Delta t) = \mathbf{v}_i(t) + \frac{\Delta t}{m_i} [\phi \mathbf{f}_i^{\text{tot},K+1}(t + \Delta t) + (1 - \phi) \mathbf{f}_i^{\text{tot}}(t)] \\ \mathbf{r}_i^{K+1}(t + \Delta t) = \mathbf{r}_i(t) + [\phi \mathbf{v}_i^{K+1}(t + \Delta t) + (1 - \phi) \mathbf{v}_i(t)] \Delta t \end{cases} \quad (30)$$

(3) CHECK FOR CONVERGENCE:

compute $\text{error}(\mathbf{r})$ and $\text{error}(\mathbf{v})$

IF ($\text{error}(\mathbf{r})$ OR $\text{error}(\mathbf{v}) > \text{TOL}$) $\Rightarrow K = K + 1$, GOTO (2) (iterate)

IF ($\text{error}(\mathbf{r})$ AND $\text{error}(\mathbf{v}) \leq \text{TOL}$) $\Rightarrow t = t + \Delta t$, GOTO (1) (move to next timestep)

Remark 4 According to (30), all velocities and positions seem to be updated only after one complete iteration. This would correspond to a Jacobi-type of scheme and is presented like so only for the sake of algebraic simplicity. What we actually do in step (2) of the algorithm is: for each particle i , we compute $\mathbf{f}_i^{\text{tot},K+1}(t + \Delta t)$ using the velocities and positions of the previous particles that have just been updated within the current iteration, that is, using $\mathbf{v}_j^{K+1}(t + \Delta t)$ and $\mathbf{r}_j^{K+1}(t + \Delta t)$, $j = 1, 2, \dots, i - 1$. For $j \geq i$, the values of the previous iteration, i.e., $\mathbf{v}_j^K(t + \Delta t)$ and $\mathbf{r}_j^K(t + \Delta t)$, are used. This resembles a Gauss–Seidel scheme, which (as it is well known) converges at a faster rate than the Jacobi method, if the Jacobi method converges, or diverges at a faster rate, if the Jacobi method diverges. For details on this subject, the reader is referred to [56].

Remark 5 The two error measures in step (3) of (30) are taken as normalized (nondimensional) measures, given, respectively, by

$$\begin{aligned} \text{error}(\mathbf{r}) &= \frac{\sum_{i=1}^{N_p} \left\| \mathbf{r}_i^{K+1}(t + \Delta t) - \mathbf{r}_i^K(t + \Delta t) \right\|}{\sum_{i=1}^{N_p} \left\| \mathbf{r}_i^{K+1}(t + \Delta t) - \mathbf{r}_i(t) \right\|} \quad \text{and} \\ \text{error}(\mathbf{v}) &= \frac{\sum_{i=1}^{N_p} \left\| \mathbf{v}_i^{K+1}(t + \Delta t) - \mathbf{v}_i^K(t + \Delta t) \right\|}{\sum_{i=1}^{N_p} \left\| \mathbf{v}_i^{K+1}(t + \Delta t) - \mathbf{v}_i(t) \right\|}. \end{aligned} \quad (31)$$

values of positions and/or velocities of particles throughout the system dynamics. To enforce the first type, rigid walls can be defined on the domain boundaries. Accordingly, any particle that shall approach these boundaries will eventually make contact with them and be bounced back to the interior of the domain. These contacts are resolved through either the overlap-based or the impulse-based model of Sect. 2, with desired contact parameters. To enforce the second type, a list of particles whose positions and/or velocities are to remain fixed throughout the solution must be given as input data in the beginning of a simulation. In such case, whenever the loop over the particles [step (2) of (30)] reaches a particle with imposed conditions, the update of the corresponding component of position and/or velocity is bypassed and the loop moves to the next component or the next particle. Alternatively, fictitious springs with very high stiffnesses can be attached to the particles whose positions and/or velocities are to remain fixed. In this case, the springs must be provided in the direction(s) that the particles are to be constrained. For the imposition of velocities, the springs have to be connected to fictitious walls and then the desired velocity is applied to the wall. The two strategies are equivalent provided that the fictitious springs of the second are stiff enough (the first, however, is clearly computationally more efficient). In this work, both have been implemented and utilized in the examples of the next section. The results are nearly indistinguishable.

5 Numerical simulations

In this section, we provide examples of numerical simulations to show how the presented framework can be used to study the deformation and rupture of membranes. We remark that it is not our intention here to provide “well-tuned” (calibrated) values for the parameters of our model, but instead just to show how the model works from a general perspective (calibration is left as a matter of separate research). We consider three different model problems for this purpose: (1) a projectile impacting a square piece of structural fabric; (2) the dynamic shearing of a square membrane; and (3) a jet of nanoparticles being shot at a lipid bi-layer. In the first problem, all particles are assumed to be relatively stiff so that the impulse-based collision scheme (Eqs. 11–14) is used; in the second and third problems, softer particles are present and thus the overlap-based collision scheme (Eqs. 8–10) is adopted.

A few comments are needed w.r.t. the parameters used in both collision models. For the overlap-based scheme, the damping constant d of Eq. (8) is taken here following the ideas of [57], which means

$$d = 2\xi \sqrt{2\sqrt{R^*E^*m^*}\delta^{1/4}}, \tag{32}$$

wherein ξ is the damping rate of the collision, which must be specified, and m^* is the effective mass of the colliding pair, i.e.,

$$m^* = \frac{m_i m_j}{m_i + m_j}. \tag{33}$$

The damping rate ξ enables one to enforce the type of energy dissipation that shall occur during the collision in the pair’s central direction. If the colliding pair is seen as one-dimensional spring–dashpot system (SDS) of mass m^* and damping rate ξ , its dynamics can be fully controlled by specifying appropriate ξ s. Recalling the solution to a vibration problem of a 1-D SDS, it follows that: (1) when $\xi = 0$, no damping exists and the collision is a perfectly elastic, energy-conserving one (undamped SDS); (2) when $0 < \xi < 1$, small-to-moderate damping exists and consequently energy dissipation occurs at small-to-moderate rates (underdamped SDS); (3) when $\xi = 1$, strong damping exists and thus rapid energy dissipation is observed (critically damped SDS); and (4) when $\xi > 1$, very strong damping with rapid dissipation is observed (overdamped SDS). Equation (32) is a generalization of the ideas proposed by Cundall and Strack [4], wherein only critically damped collisions were considered.

The overlap-based model requires that the collisions be resolved with small time-steps, such that both δ and $\dot{\delta}$ be accurately computed. Here, we select Δt so as to ensure at least ten time steps per collision, estimating the duration of

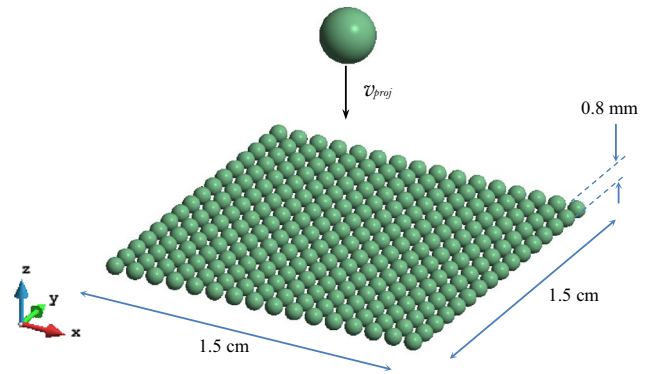


Fig. 3 Projectile impacting a structural fabric

a typical collision by means of the Hertz’s formula for elastic collisions [48], which means

$$\text{duration} \cong 2.87 \left(\frac{m^*}{R^*(E^*)^2 v_{\text{rel}}} \right)^{1/5} \Rightarrow \Delta t \leq \frac{\text{duration}}{10}, \tag{34}$$

where v_{rel} is the relative velocity of the colliding pair in the pair’s central direction at the beginning of the collision. The natural frequencies of the membrane springs, given approximately by $\sqrt{k_{ij}/m^*}$, must also be checked against (34), in order to avoid poor capturing of the springs vibrations. These considerations lead invariably to small time-step sizes, which implies that the explicit version ($\phi = 0$) of our time integration scheme is preferred for this cases (an implicit integration would be highly inefficient since it would perform iterations no matter how small or big Δt is).

For the impulse-based scheme, in its turn, we adopt $\delta t = 0.01\Delta t$ for the collisions’ durations, and use the implicit version of the integration scheme, with $\phi = 0.5$ and Δt dictated solely by the natural frequencies of the membrane springs.

5.1 Projectile impacting a structural fabric

A spherical projectile of radius $R_{\text{proj}} = 1.25$ mm is shot at a flat, mono-layer piece of structural fabric of side dimensions 1.5×1.5 cm² and thickness 0.8 mm, as depicted in Fig. 3. The fabric is held fixed at its four edges and is pre-stretched on both directions before the projectile is shot, with initial strains $\epsilon_{0x} = \epsilon_{0y} = 11$ %. It is idealized as a single layer of particles arranged in a regular pattern with no cross-wise springs, similar to what was shown in Fig. 2. Two different shots are considered: one for which $v_{\text{proj}} = 100$ m/s, and another for which $v_{\text{proj}} = 300$ m/s. Other data are as follows:

- Mass density of the projectile: $\rho_{\text{proj}} = 2,500$ kg/m³;
- Mass density of the fabric: $\rho_{\text{fabr}} = 2,000$ kg/m³

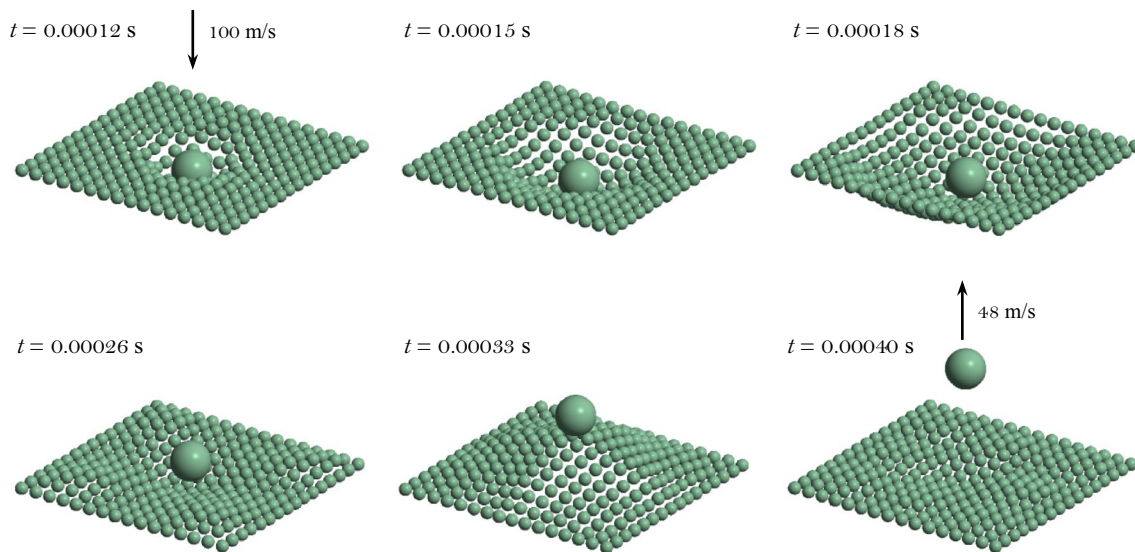


Fig. 4 Projectile impacting a structural fabric. Simulations results for shot of 100 m/s

- Radius of the fabric particles: $R_{\text{fabr}} = 0.4$ mm;
- Initial distance between centers of neighboring fabric particles on both x and y directions: 1 mm;
- Stiffness constant for the fabric springs:
 $k_{ij} = 2.5 \times 10^4$ N/m;
- Dashpot constant for the fabric dashpots:
 $c_{ij} = 0.00015$ Ns/m;
- Critical strain for fabric rupture: $\varepsilon_{ij}^{\text{crit}} = 15$ %;
- Coefficient of restitution for impulse-based collisions:
 $e = 0.9$;
- Coefficient of dynamic friction: $\mu_d = 0.1$;
- Environment drag force parameters:
 $c_{\text{env}} = 0.00005$ Ns/m and $\mathbf{v}_{\text{env}} = \mathbf{o}$;
- Gravity and fluid pressure forces are neglected ($\mathbf{g} = \mathbf{o}$ and $\mathbf{f}_i^{\text{pres}} = \mathbf{o}$);
- Time step size: $\Delta t = 5 \times 10^{-8}$ s;
- Final time at the end of the simulation: $t_{\text{final}} = 0.001$ s.

Figures 4 and 5 depict a sequence of snapshots, at selected time instants, of deformed configurations obtained in the simulations for the cases of $v_{\text{proj}} = 100$ and 300 m/s, respectively. Therein one can see the progression of the fabric deformation with the impact of the projectile. Notice that the fabric was able to endure the impact without experiencing any damage in the case where $v_{\text{proj}} = 100$ m/s. Moreover, after the projectile's energy was absorbed (and partly dissipated), the fabric recovered its initial shape while the projectile rebounded backwards with a lower velocity (~ 48 m/s) as compared to its original shooting speed. For the case in which $v_{\text{proj}} = 300$ m/s, the projectile broke the SDs and fully penetrated the fabric, emerging at its opposite face with $v_{\text{proj}} = 238$ m/s (some energy is thus absorbed by the fabric in this case).

It should be noticed how the proposed framework is capable of handling multiple contact/impact with the opening of localized “holes” on the fabric, through which incoming objects are occasionally able to pass. This would be very difficult to resolve using other approaches, e.g., continuum (instead of discrete) theories and their accompanying spatial discretizations. Parametric studies, varying the projectile's velocity, mass and diameter, and also the fabric's thickness and stiffnesses, could be readily conducted with these types of computational simulation. This can be very useful in the optimum design of fabrics and projectiles.

5.2 Dynamic shearing of a square membrane

A squared flat membrane of side dimensions 4.0×4.0 cm² and thickness 0.8 mm has two of its opposite edges mounted into rigid walls, the other two being fully unrestrained as indicated in Fig. 6. One of the walls is held still while the other is given a lateral constant velocity $v_{\text{wall}} = 50.0$ m/s, causing the membrane to undergo an in-plane (dynamic) shearing deformation. Before motion is set forth, the membrane is pre-stretched in the direction perpendicular to v_{wall} , with an initial strain of $\varepsilon_{0y} = 2.0$ %. A regular pattern of particles is adopted to represent the membrane, using both rectangular-gridded and cross-wised SDs to connect the particles.

Other data are as follows:

- Mass density of the membrane: $\rho_{\text{membr}} = 2,000$ kg/m³;
- Radius of the membrane particles: $R_{\text{membr}} = 0.4$ mm;
- Distance between centers of neighboring particles on both x and y directions: 1 mm;

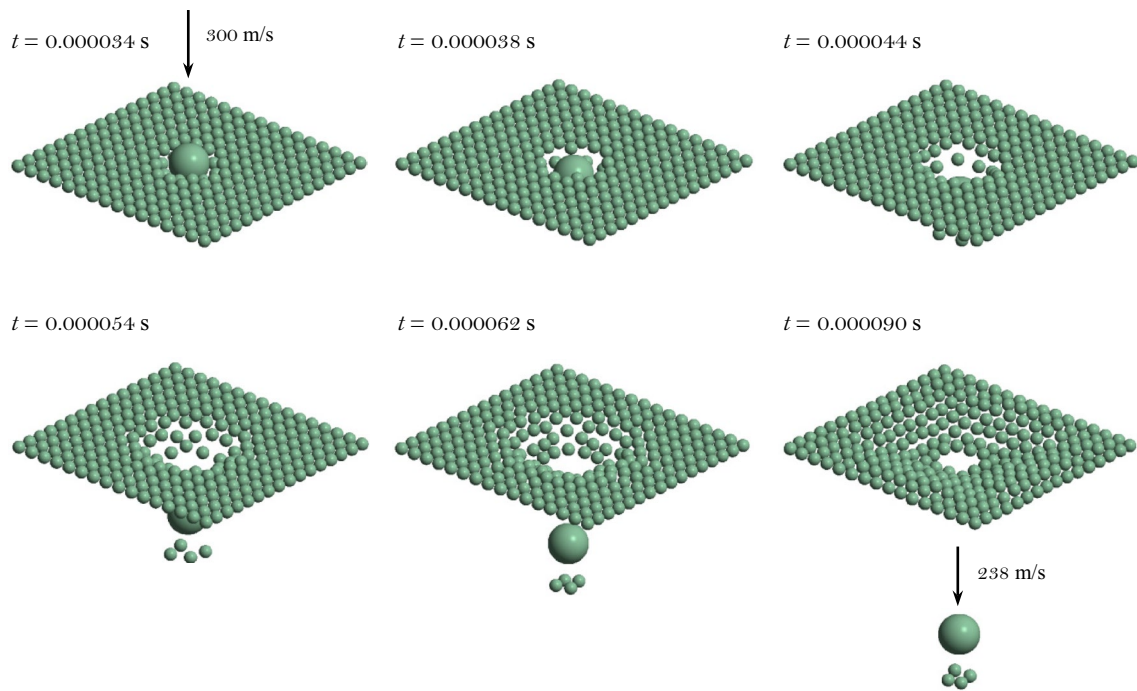


Fig. 5 Projectile impacting a structural fabric. Simulations results for shot of 300 m/s

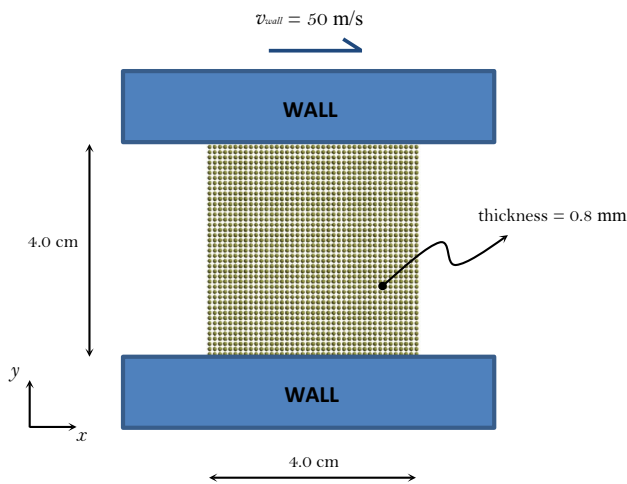


Fig. 6 Dynamic shearing of a square membrane

- SD constants (rectangular grid): $k_{ij}^{rec} = 20 \text{ N/m}$ and $c_{ij}^{rec} = 0.00002 \text{ Ns/m}$;
- SD constants (cross-wise): $k_{ij}^{cw} = 0.5 \text{ N/m}$ and $c_{ij}^{cw} = 0.00012 \text{ Ns/m}$;
- Critical strain for membrane rupture (for all SDs): $\varepsilon_{ij}^{crit} = 25 \%$;
- Elastic properties of membrane particles (needed for overlap-based collisions): $E = 1.0 \times 10^6 \text{ N/m}^2$ and $\nu = 0.25$;
- Damping rate for overlap-based collisions: $\xi = 0.1$;

- Coefficient of dynamic friction: $\mu_d = 0.1$;
- Environment drag force parameters: $c_{env} = 0.00002 \text{ Ns/m}$ and $v_{env} = \mathbf{o}$;
- Gravity and fluid pressure forces are neglected ($\mathbf{g} = \mathbf{o}$ and $\mathbf{f}_i^{pres} = \mathbf{o}$);
- Time step size: $\Delta t = 5 \times 10^{-6} \text{ s}$;
- Final time at the end of the simulation: $t_{final} = 0.0004 \text{ s}$.

Figure 7 depicts snapshots of deformed configurations (at arbitrary time instants) that were obtained in the simulation. One can notice the severe shearing experienced by the membrane, which (as expected) is accompanied by tensile and compressive strains in the directions of the membrane’s diagonals. At the end of the simulation, the total lateral displacement imposed by the moving wall was $\Delta L_x = 2.0 \text{ cm}$. No rupture was observed in this case. Also, no out-of-plane displacements (corresponding to the formation of wrinkles due to localized compressive stresses) were seen. This is because transverse loadings or imperfections were not introduced in the problem. The modeling of wrinkles within the framework that is proposed here is a matter of current research by the author and will be presented in a forthcoming work.

5.3 Jet of nanoparticles impinging a lipid bi-layer

Lipid bi-layers consist of an assembly of lipid molecules organized into membrane-like (i.e., bi-dimensional) two-layered structures due to amphiphilic effects (the phosphoric

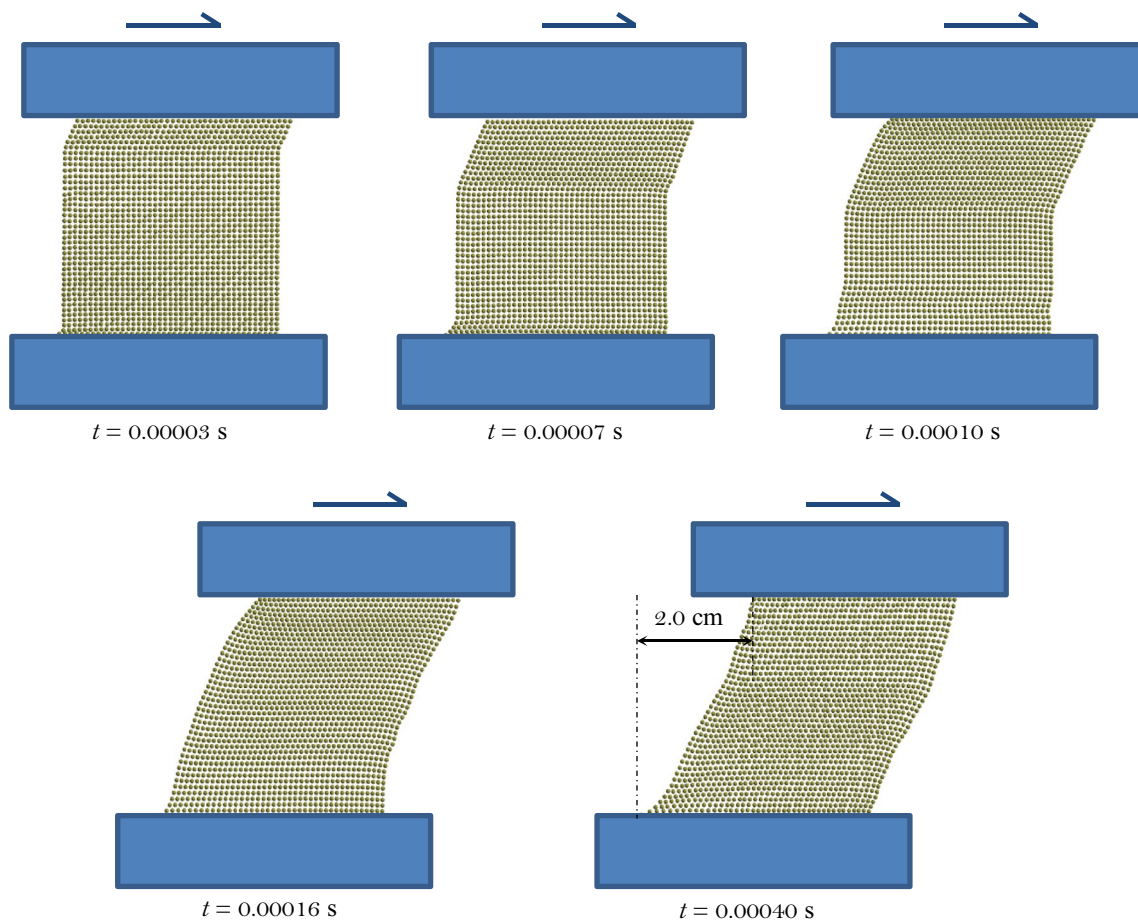


Fig. 7 Dynamic shearing of a square membrane: simulation results (sequence is from left to right, top to down)

headgroups of the lipids are hydrophilic, the hydrocarbon chains are hydrophobic). The forces that held these molecules together arise from weaker van der Waals, hydrophobic and hydrogen-bonding interactions, providing the structure a very soft, flexible (almost fluid-like) behavior, and yet, a good response to both stretching and bending deformations. In this example, we consider the shooting of a lipid bi-layer by a jet of nanoparticles at a high incoming velocity. We idealize each lipid of a layer as a spherical particle (corresponding to the lipid phosphoric headgroup) that is bonded to its neighboring ones of the same layer by means of in-plane (rectangular-gridded) SDs. The “piled layers” scheme that was mentioned in Sect. 3 is then invoked to form the bi-layer, whereby transverse (through-the-thickness) SDs are used to connect the two layers together. Within this setting, a square bi-layer of side dimensions $39.0 \times 39.0 \text{ nm}^2$ and thickness 5.0 nm is considered, the diameter of its lipid particles being taken as $\phi_{\text{lipid}} = 2.5 \text{ nm}$. Its four edges are assumed to be fixed. A jet of particles, each with diameter $\phi_{\text{jet}} = 1.25 \text{ nm}$ and velocity $v_{\text{jet}} = 100 \text{ m/s}$, is shot at the bi-layer. The problem is as illustrated in Fig. 8 (all dimensions shown are from center to center of particles).

We assume that there exists a pressure gradient from the bottom to the top sides of the bi-layer, which leads to an upward pressure force $f_i^{\text{pres}} = f_i^p \mathbf{v}_i$ on each particle of the lower layer (here, f_i^p is the intensity of the force and \mathbf{v}_i is the local normal direction at particle i of the lower layer, pointing upwards). Direction \mathbf{v}_i is computed for each particle of the lower layer by taking successive cross-products involving the particle’s position vector \mathbf{r}_i and its immediate neighboring ones \mathbf{r}_{i-1} and \mathbf{r}_{i+1} of the same layer, and then normalizing the result. The pressure force is a live load, in the sense that it changes its direction as the bi-layer deforms due to the impact of the jet, and therefore each local direction \mathbf{v}_i has to be recomputed at every iteration and new time step. The intensity f_i^p , however, is kept here as constant for the sake of simplicity. We assume that the jet particles do not experience any pressure forces (but do experience drag, whose intensity is shown below). The other data for the problem are as follows:

- Mass density of the jet particles = $1,800 \text{ kg/m}^3 = 1.8 \times 10^{-6} \text{ fg/nm}^3$;
- Mass density of the bi-layer = $900 \text{ kg/m}^3 = 9 \times 10^{-7} \text{ fg/nm}^3$;

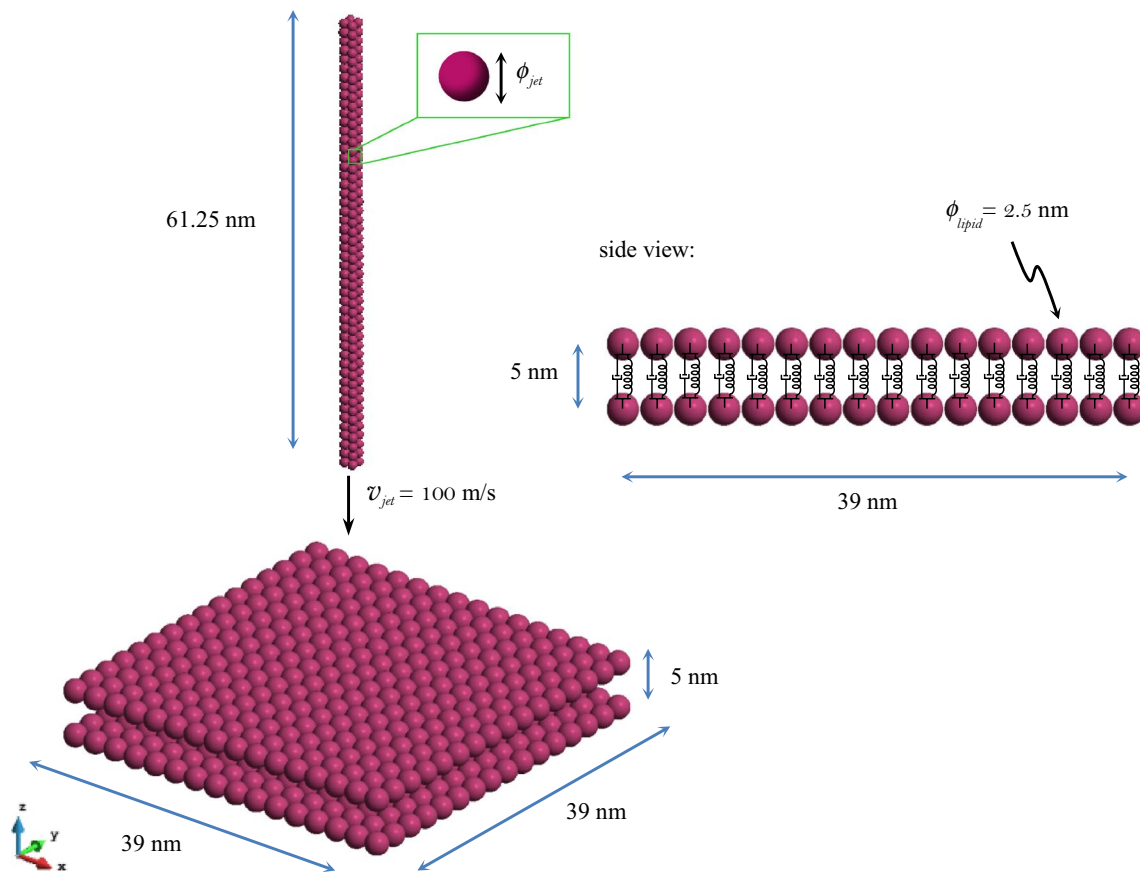


Fig. 8 Jet of nanoparticles impinging a lipid bi-layer

- Spring constant for the SDs: $k_{ij} = 4 \times 10^{-3}$ nN/nm;
- Dashpot constant for SDs: $c_{ij} = 0.00001$ nN ns/nm;
- Critical strain for springs rupture: $\varepsilon_{crit} = 0.5$;
- Elastic properties of jet and lipid particles (needed for overlap-based collisions): $E_{jet} = E_{lipid} = 100$ nN/nm² and $v_{jet} = v_{lipid} = 0.25$;
- Damping rate for overlap-based collisions: $\xi = 0.1$;
- Coefficient of dynamic friction: $\mu_d = 0.1$;
- Pressure gradient force magnitude: $f_i^p = 6.5 \times 10^{-6}$ nN;
- Drag force parameters: $c_{env} = 0.000005$ nN ns/nm and $v_{env} = \mathbf{o}$;
- Gravity is neglected ($\mathbf{g} = \mathbf{o}$);
- Time step size = 0.0002 ns;
- Final time at the end of the simulation = 5 ns.

Figure 9 depicts a sequence of deformed configurations obtained in the analysis. Therein one can see the gradual penetration of several jet particles of the jet. At the end of the simulation, 156 jet particles (from a total of 200) were observed to have penetrated the bi-layer. This lead to a “delivery” rate (defined as the ratio of the number of jet particles that penetrated to the total number of jet particles) of 78 %. Interestingly, a few particles ended

trapped between the two layers, what could be a desired effect in some applications. Notice that the bi-layer was able to endure the impact of the jet without experiencing any damage in this case. Moreover, after the jet energy was absorbed (and partly dissipated), the bi-layer recovered its initial shape while enclosing the “delivered” particles under its bottom surface. Once more, it can be seen that the proposed framework is able to handle multiple contact/impact with the opening of localized “holes” on the membrane, through which incoming particles are occasionally able to pass. We again emphasize that this would be very difficult to resolve using other approaches (e.g., continuum theories and their accompanying spatial discretization).

For more detailed aspects about lipid membranes and their behavior, the reader is referred to the works of [40, 47], and the many references therein.

6 Closing remarks and future work

The main purpose of this work was to present a simple computational framework for the simulation of rupture on membranes and thin films. It is grounded on a

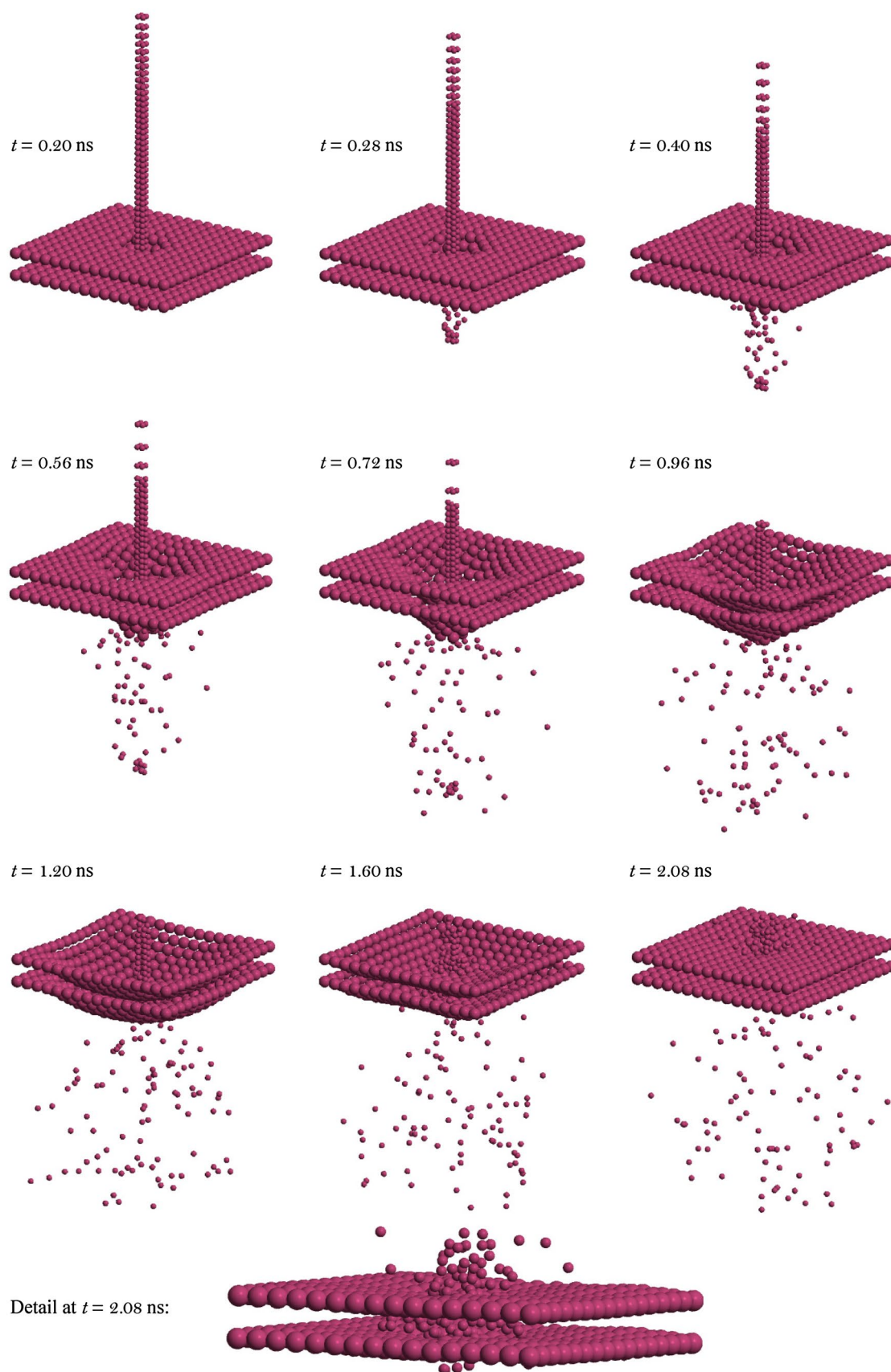


Fig. 9 Jet of nanoparticles impinging a lipid bi-layer: simulation results (sequence is from *left to right, top to down*)

particle-based (discrete element) method and can be numerically implemented with small effort by researchers interested in these problems. The main advantages of such an approach are that (1) both quasistatic and dynamic rupture can be satisfactorily represented with only very simple descriptions of the underlying microstructure of the membrane or thin film, and (2) such different systems as structural fabrics, thin biological tissues and lipid membranes can be modeled under the same general framework. Multiple contact/impact with localized rupture is straightforward to characterize.

We remark that the purpose here was simply to show how the approach works from a general perspective. Evidently, for specific applications, more specific features need to be incorporated, and better values for its numerical parameters need to be considered (e.g., calibrated against experimental data). One can render, for example, the presence of electric charges relevant to a certain problem and then incorporate electrostatic forces of the type of Coulombic interactions, by adding the term

$$f_i^{elec} = \sum_{j=1, j \neq i}^{N_p} \frac{q_i q_j}{4\pi \epsilon \|\mathbf{r}_i - \mathbf{r}_j\|^2} \mathbf{n}_{ij} \tag{35}$$

to the particle’s total force vector (in this case, q_i and q_j are the electric charges of particles i and j and ϵ is the permittivity). Likewise, the presence of external electric and/or magnetic fields may be considered, by taking them as environmental effects and adding the contributions $q_i \mathbf{E}$ (\mathbf{E} = electric field) and $q_i \mathbf{v}_i \times \mathbf{B}$ (\mathbf{B} = magnetic field) to the particles’ environment force vector. These fields can be used to temporarily modify the membrane’s mechanical response such that stretching and/or compressing is facilitated or hindered.

In general, coupled multifield approaches are necessary to more realistically simulate complex membrane problems. For example, the deformation response of the membrane can be dependent on the local temperature T . One can take this into account within our framework by assuming $k_{ij} = \hat{k}(\Delta L_{ij}, T_{ij})$ for the springs, wherein the evolution of T_{ij} is described by a corresponding differential equation that must also be resolved in the time integration scheme. Or, the rupture response can be dependent on the accumulated local damage (instead of the abrupt rupture as assumed here), what can be accounted for by coupling a one-dimensional damage model to the expression of the spring force. This can encompass the use of a scalar damage variable α , $0 \leq \alpha \leq 1$, such that for a totally undamaged spring one has $\alpha = 1$, whereas for a totally damaged one $\alpha = 0$. The evolution of α with respect to the spring’s elongation has to be described by some given law (one possible simple representation is as proposed by [15] for fibrous biological tissues).

As further steps to the use of the framework proposed here, one may attempt to (1) post-process detailed statistical information on simulation results (define figures of merit for the problem at hand and compute their various moments); (2) develop more ad hoc constitutive laws for the spring forces, and (3) devise a coupled (multifield) time integration scheme to account for the above-mentioned thermal and damage effects, and also to allow for a more realistic representation of the surrounding fluid (fully coupled fluid-particle interaction). We believe that particle-based models can be a very useful approach to study the rupture of membranes and thin films.

Acknowledgments This work was supported by FAPESP (Fundação de Amparo à Pesquisa do Estado de São Paulo), under the Grant 2012/04009-0 (which made possible a research stay for the author at the University of California at Berkeley, on a momentary leave from the University of São Paulo), and by CNPq (Conselho Nacional de Desenvolvimento Científico e Tecnológico), under the Grant 303793/2012-0. Material support and the stimulating discussions in CMRL (Computational Materials Research Laboratory, UC Berkeley) are also gratefully acknowledged.

Appendix

For two colliding particles i and j , a balance of linear momentum in the particles’ central direction relating the states immediately before (time instant t^*) and after (time instant $t^* + \delta t$) impact renders

$$m_i v_{in}(t^*) + m_j v_{jn}(t^*) + \int_{t^*}^{t^* + \delta t} \mathbf{f}_i \cdot \mathbf{n}_{ij} dt + \int_{t^*}^{t^* + \delta t} \mathbf{f}_j \cdot \mathbf{n}_{ij} dt = m_i v_{in}(t^* + \delta t) + m_j v_{jn}(t^* + \delta t), \tag{36}$$

in which subscript n denotes component in the direction of \mathbf{n}_{ij} [see Eq. (13)] and \mathbf{f}_i and \mathbf{f}_j are, respectively, the sum of all forces that act on particle i and particle j during the collision except for the pair’s contact force itself, i.e.,

$$\begin{aligned} \mathbf{f}_i &= \mathbf{f}_i^{env} + \mathbf{f}_i^{memb} + \sum_{k \neq j} \mathbf{f}_{ik}^{con} + \mathbf{f}_i^{fric} \quad \text{and} \\ \mathbf{f}_j &= \mathbf{f}_j^{env} + \mathbf{f}_j^{memb} + \sum_{k \neq i} \mathbf{f}_{jk}^{con} + \mathbf{f}_j^{fric}. \end{aligned} \tag{37}$$

We can write such a balance for each isolated particle as well, what for particle i leads to

$$m_i v_{in}(t^*) + \int_{t^*}^{t^* + \delta t} \mathbf{f}_i \cdot \mathbf{n}_{ij} dt + \int_{t^*}^{t^* + \delta t} I_n dt = m_i v_{in}(t^* + \delta t), \tag{38}$$

where the second integral on the left side of the equation amounts to the total impulse that particle i receives from particle j due to impact in the pair’s central direction. The collision event can be decomposed into a compression and a recovery phase, with corresponding durations δt_1 and δt_2 , respectively, such that $\delta t = \delta t_1 + \delta t_2$. In

the instant of transition from one phase to the other (i.e., instant $t^* + \delta t_1$), the relative velocity of the particles in the direction of \mathbf{n}_{ij} turns to zero, meaning that the pair attains a common velocity v_{cn} in this direction. Accordingly, Eq. (38) can be decomposed into each one of these phases, yielding

$$m_i v_{in}(t^*) + \int_{t^*}^{t^* + \delta t_1} \mathbf{f}_i \cdot \mathbf{n}_{ij} dt + \int_{t^*}^{t^* + \delta t_1} I_n dt = m_i v_{cn} \quad (39)$$

for the compression phase and

$$m_i v_{cn} + \int_{t^* + \delta t_1}^{t^* + \delta t} \mathbf{f}_i \cdot \mathbf{n}_{ij} dt + \int_{t^* + \delta t_1}^{t^* + \delta t} I_n dt = m_i v_{in}(t^* + \delta t) \quad (40)$$

for the recovery phase. Similarly, for particle j one writes

$$m_j v_{jn}(t^*) + \int_{t^*}^{t^* + \delta t_1} \mathbf{f}_j \cdot \mathbf{n}_{ij} dt - \int_{t^*}^{t^* + \delta t_1} I_n dt = m_j v_{cn} \quad (41)$$

and

$$m_j v_{cn} + \int_{t^* + \delta t_1}^{t^* + \delta t} \mathbf{f}_j \cdot \mathbf{n}_{ij} dt - \int_{t^* + \delta t_1}^{t^* + \delta t} I_n dt = m_j v_{jn}(t^* + \delta t). \quad (42)$$

Equations (39) and (40), or equivalently, (41) and (42), provide a means to compute the impulses that each particle receives from the other in the compression and recovery phases in the pair’s central direction. The ratio between these impulses is the coefficient of restitution e of the colliding pair, which is a specified (given) quantity:

$$e = \frac{\int_{t^* + \delta t_1}^{t^* + \delta t} I_n dt}{\int_{t^*}^{t^* + \delta t_1} I_n dt}. \quad (43)$$

By inserting (39) and (40) [or equivalently, (41) and (42)] into (43), one arrives at

$$e = \frac{m_i(v_{in}(t^* + \delta t) - v_{cn}) - I_{f_i}^{rec}}{m_i(v_{cn} - v_{in}(t^*)) - I_{f_i}^{comp}} = \frac{-m_j(v_{jn}(t^* + \delta t) - v_{cv}) + I_{f_j}^{rec}}{-m_j(v_{cn} - v_{jn}(t^*)) + I_{f_j}^{comp}}, \quad (44)$$

where

$$I_{f_i}^{rec} = \int_{t^* + \delta t_1}^{t^* + \delta t} \mathbf{f}_i \cdot \mathbf{n}_{ij} dt, \quad I_{f_i}^{comp} = \int_{t^*}^{t^* + \delta t_1} \mathbf{f}_i \cdot \mathbf{n}_{ij} dt, \\ I_{f_j}^{rec} = \int_{t^* + \delta t_1}^{t^* + \delta t} \mathbf{f}_j \cdot \mathbf{n}_{ij} dt \quad \text{and} \quad I_{f_j}^{comp} = \int_{t^*}^{t^* + \delta t_1} \mathbf{f}_j \cdot \mathbf{n}_{ij} dt \quad (45)$$

are the impulses due to \mathbf{f}_i and \mathbf{f}_j in the pair’s central direction during the recovery and compressive phases. Since v_{cn} is present on both forms of (44), it can be eliminated, leading to

$$e = \frac{v_{jn}(t^* + \delta t) - v_{in}(t^* + \delta t) + \Delta_{ij}^{rec}}{v_{in}(t^*) - v_{jn}(t^*) + \Delta_{ij}^{comp}}, \quad (46)$$

in which

$$\Delta_{ij}^{rec} = \frac{1}{m_i} I_{f_i}^{rec} - \frac{1}{m_j} I_{f_j}^{rec} \quad \text{and} \quad \Delta_{ij}^{comp} = \frac{1}{m_i} I_{f_i}^{comp} - \frac{1}{m_j} I_{f_j}^{comp}. \quad (47)$$

Equation (46) furnishes an expression for $v_{jn}(t^* + \delta t)$, which can in turn be inserted into the pair’s Eq. (36). By doing so, and considering the definition of the (averaged) resultant force that acts on particle i during the collision given by Eq. (14), and the equivalent definition for the (averaged) resultant force that acts on particle j , the following result is attained

$$v_{in}(t^* + \delta t) = \frac{m_i v_{in}(t^*) + m_j(v_{jn}(t^*) - e(v_{in}(t^*) - v_{jn}(t^*)))}{m_i + m_j} + \frac{(\bar{f}_{in} + \bar{f}_{jn})\delta t - m_j(e\Delta_{ij}^{comp} - \Delta_{ij}^{rec})}{m_i + m_j}. \quad (48)$$

Once $v_{in}(t^* + \delta t)$ is known, one can subsequently obtain $v_{jn}(t^* + \delta t)$ via Eq. (46). Finally, having the post-collision velocities, the total impulse that particle i receives from particle j due to impact in the pair’s central direction can be computed with the aid of Eq. (38) (or its equivalent counterpart for particle j), yielding

$$\int_{t^*}^{t^* + \delta t} I_n dt = m_i(v_{in}(t^* + \delta t) - v_{in}(t^*)) - \int_{t^*}^{t^* + \delta t} \mathbf{f}_i \cdot \mathbf{n}_{ij} dt, \quad (49)$$

which leads to the (averaged) impulsive force given by Eq. (12).

References

1. Crowe CT, Schwarzkopf JD, Sommerfeld M, Tsuji Y (2012) Multiphase flows with droplets and particles. CRC Press, Boca Raton
2. Pöschel T, Schwager T (2004) Computational granular dynamics. Springer, Berlin
3. Duran J (1997) Sands, powders and grains: an introduction to the physics of granular matter. Springer, New York
4. Cundall P, Strack O (1979) A discrete numerical model for granular assemblies. Geotechnique 29(1):47–65
5. David CT, Garcia-Rojo R, Herrmann HJ, Luding S (2007) Powder flow testing with 2D and 3D biaxial and triaxial simulations. Part Part Syst Charact 24:29–33
6. Kamrin K, Koval G (2014) Effect of particle surface friction on nonlocal constitutive behavior of flowing granular media. Comput Part Mech 1:169–176
7. Kroupa M, Klejch M, Vonka M, Kosek J (2012) Discrete element modeling (DEM) of agglomeration of polymer particles. Proc Eng 42:58–69
8. Bolintineanu DS, Grest GS, Lechman JB, Pierce F, Plimpton SJ, Schunk PR (2014) Particle dynamics modeling methods for colloid suspensions. Comput Part Mech 1(3):321–356

9. Tan Y, Yang D, Sheng Y (2009) Discrete element method (DEM) modeling of fracture and damage in the machining process of polycrystalline SiC. *J Euro Ceram Soc* 29(6):1029–1037
10. Zohdi TI (2009) Mechanistic modeling of swarms. *Comput Methods Appl Mech Eng* 198(21–26):2039–2051
11. Bicanic N (2004) Discrete element methods. In: Stein E, de Borst R, Hughes TJR (eds) *Encyclopedia of computational mechanics, vol 1: fundamentals*. Wiley, Chichester
12. Zhu HP, Zhou ZY, Yang RY, Yu AB (2008) Discrete particle simulation of particulate systems: a review of major applications and findings. *Chem Eng Sci* 63:5728–5770
13. O’Sullivan C (2011) Particle-based discrete element modeling: geomechanics perspective. *Int J Geomech* 11:449–464
14. Zohdi TI, Powell D (2006) Multiscale construction and large-scale simulation of structural fabric undergoing ballistic impact. *Comput Methods Appl Mech Eng* 195:94–109
15. Zohdi TI (2007) A computational framework for network modeling of fibrous biological tissue deformation and rupture. *Comput Methods Appl Mech Eng* 196:2972–2980
16. Zohdi TI (2010) High-speed impact of electromagnetically sensitive fabric and induced projectile spin. *Comput Mech* 46:399–415
17. Mseis GN, Zohdi TI (2011) Micromechanical modeling and numerical simulation of chain-mail armor. *Int J Fract* 170:183–190
18. Zohdi TI (2010) On the dynamics of charged electromagnetic particulate jets. *Arch Comp Methods Eng* 17(2):109–135
19. Valdés JG, Miguel J, Oñate E (2009) Nonlinear finite element analysis of orthotropic and pre-stressed membrane structures. *Finite Elem Anal Des* 45(6–7):395–405
20. Gama BA, Gillespie JW Jr (2011) Finite element modeling of impact, damage evolution and penetration of thick-section composites. *Int J Impact Eng* 38(4):181–197
21. Chaouachia F, Rahalia Y, Ganghoffer JF (2014) A micromechanical model of woven structures accounting for yarn–yarn contact based on Hertz theory and energy minimization. *Compos B Eng* 66:368–380
22. Tong G, Liu TF (2013) Finite element analysis of woven fabric laminates structural strength. *Adv Mater Res* 785–786:199–203
23. Lin H, Clifford MJ, Long AC, Lee K, Guo N (2012) A finite element approach to the modelling of fabric mechanics and its application to virtual fabric design and testing. *J Text Inst* 103(10):1063–1076
24. Pauletti RMO (2010) Some issues on the design and analysis of pneumatic structures. *Int J Struct Eng* 1:217–240
25. Deng X, Pellegrino S (2012) Wrinkling of orthotropic viscoelastic membranes. *AIAA J* 50(3):668–681
26. Gonçalves FR, Campello EMB (2014) Orthotropic material models for the computational modeling of structural membranes. *J Braz Soc Mech Sci Eng* 36:887–899
27. Philipp B, Bletzinger K-U (2013) Hybrid Structures – Enlarging the Design Space of Architectural Membranes. *J Int Assoc Shell Spat Struct* 54(4):281–291
28. Jiménez FL, Pellegrino S (2013) Failure of carbon fibers at a crease in a fiber-reinforced silicone sheet. *J Appl Mech* 80(1):011020
29. Holzapfel GA (2001) Biomechanics of soft tissue. In: Lemaitre J (ed) *The handbook of materials behavior models, multiphysics behaviors, composite media, biomaterials, vol III*. Academic Press, Boston
30. Humphrey JD (2003) Continuum biomechanics of soft biological tissues. *Proc R Soc* 459(2029):3–46
31. Rausch MK, Kuhl E (2013) On the effect of prestrain and residual stress in thin biological membranes. *J Mech Phys Solids* 61(9):1955–1969
32. Atai A, Steigmann DJ (2012) Modeling and simulation of sutured biomembranes. *Mech Res Commun* 46:34–40
33. Wang Y, Sigurdsson JK, Brandt E, Atzberger PJ (2013) Dynamic implicit-solvent coarse-grained models of lipid bilayer membranes: Fluctuating hydrodynamics thermostat. *Phys Rev E* 88:023301-1-5
34. Delemotte L, Tarek M (2012) Molecular dynamics simulations of lipid membrane electroporation. *J Membr Biol* 245(9):531–543
35. Andoh Y, Okazaki S, Ueoka R (2013) Molecular dynamics study of lipid bilayers modeling the plasma membranes of normal murine thymocytes and leukemic GRS1 cells. *Biochim Biophys Acta* 1828(4):1259–1270
36. Campello EMB, Zohdi TI (2014) A computational framework for simulation of the delivery of substances into cells. *Int J Numer Methods Biomed Eng*. doi:10.1002/cnm.2649
37. Campello EMB, Zohdi TI (2014) Design evaluation of a particle bombardment system used to deliver substances into cells. *Comput Model Eng Sci* 98(2):221–245
38. Hac AE, Seeger HM, Fidorra M, Heimburg T (2005) Diffusion in two-component lipid membranes—a fluorescence correlation spectroscopy and monte carlo simulation study. *Biophys J* 88:317–333
39. Marrink SJ, Vries AH, Mark AE (2004) Coarse grained model for semiquantitative lipid simulations. *J Phys Chem B* 108(2):750–760
40. Roiter Y, Ornatska M, Rammohan AR, Balakrishnan J, Heine DR, Minko S (2008) Interaction of nanoparticles with lipid membrane. *Nano Lett* 8(3):941–944
41. Khelashvili G, Weinstein H, Harries D (2008) Protein diffusion on charged membranes: a dynamic mean-field model describes time evolution and lipid reorganization. *Biophys J* 94:2580–2597
42. Rangamani p, Agrawal A, Mandadapu KK, Oster G, Steigmann D (2013) Interaction between surface shape and intra-surface viscous flow on lipid membranes. *Biomech Model Mechanobiol* 12:833–845
43. Zohdi TI (2012) *Dynamics of charged particulate systems: modeling, theory and computation*. Springer, New York
44. Pijush KK, Cohen IM, Dowling DR (2012) *Fluid mechanics*. Elsevier, Oxford
45. Lennard-Jones JE (1924) On the determination of molecular fields. *Proc R Soc Lond A* 106(738):463–477
46. Johnson KL, Kendall K, Roberts AD (1971) Surface energy and the contact of elastic solids. *Proc R Soc Lond A* 324:301–313
47. Israelachvili JN (2011) *Intermolecular and surface forces*. Elsevier, Amsterdam
48. Johnson KL (1985) *Contact mechanics*. Cambridge University Press, Cambridge
49. Ramachandran A, Anderson TH, Leal LG, Israelachvili JN (2011) Adhesive interactions between vesicles in the strong adhesion limit. *Langmuir* 27:59–73
50. Pavinatto FJ, Pavinatto A, Caseli L, dos Santos Jr DS, Nobre TM, Zaniquelli MED, Oliveira ON Jr (2007) Interaction of chitosan with cell membrane models at the air–water interface. *Biomacromolecules* 8:1633–1640
51. Jähnig F (1996) What is the surface tension of a lipid bilayer membrane? *Biophys J* 71:1348–1349
52. Pipkin AC (1986) The relaxed energy density for isotropic elastic membranes. *IMA J Appl Math* 36:297–308
53. Steigmann DJ (1990) Tension field theory. *Proc R Soc Lond A* 429:141–173
54. Atai AA, Steigmann DJ (1998) Coupled deformations of elastic curves and surfaces. *Int J Solids Struct* 35:1915–1952
55. Zohdi TI (2007) *Introduction to the modeling and simulation of particulate flows*. SIAM, Berkeley
56. Axelsson A (1994) *Iterative solution methods*. Cambridge University Press, Cambridge
57. Wellmann C, Wriggers P (2012) A two-scale model of granular materials. *Comput Methods Appl Mech Eng* 205–208:46–58